To be submitted to
Physical Review B

ISTITUTO NAZIONALE DI FISICA NUCLEARE
Laboratori Nazionali di Frascati

LNF-84/23(P)
19 Aprile 1984

A. Balzarotti, A. Kisiel, N. Motta, M. Zimnal-Starnawska, M. T. Czyzyk and M. Podgorny: A MODEL OF THE LOCAL STRUCTURE OF RANDOM TERNARY ALLOYS: EXPERIMENT VERSUS THEORY.

Servizio Documentazione
dei Laboratori Nazionali di Frascati
Cas. Postale 13 - Frascati (Roma)

INFN - Laboratori Nazionali di Frascati
Servizio Documentazione

LNF-84/23(P)
19 Aprile 1984

A MODEL OF THE LOCAL STRUCTURE OF RANDOM TERNARY ALLOYS: EXPERIMENT VERSUS THEORY

A. Balzarotti(+), A. Kisiel(x), N. Motta(+), M. Zimnal-Starnawska(x)
INFN - Laboratori Nazionali di Frascati, Gruppo PULS
and
(+) Dipartimento di Fisica dell'Università di Roma II,
(x) Institute of Physics, Jagiellonian University, Cracow, Poland

M. T. Czyzyk
Institute of Physics, Theoretical Solid Stata Group of the General Physics Department, Jagiellonian University, Cracow, Poland

M. Podgorny(x)
Institut für Physik, Dortmunt Universität, Dortmunt, W. Germany

ABSTRACT

We have performed an extended X-ray absorption fine structure measurement of $Cd_{1-x}Mn_xTe$ solid solution for various concentrations x in the single phase range $0 \leq x \leq 0.7$. Data have been collected on the Mn, K, Cd L_{III} and Te L_{III} edges. We have found well-defined different nearest-neighbor Cd-Te and Mn-Te distances almost independent of x. We have developed a model of the microscopic structure of the zinc-blende-type $A_{1-x}B_xC$ ternary alloys based on a random distribution of cations. The model describes the bimodal distribution of near-neighbor distances in terms of distortion of the anion sublattice using only the lattice constant of the alloy and the bond-stretching constants of each binary component. Its application to $Cd_{1-x}Mn_xTe$ and $In_{1-x}Ga_xAs$ alloys proved to be in excellent agreement with the EXAFS results. Within the framework of this model we consider also the problem of the structural stability of $Cd_{1-x}Mn_xTe$.

(x) - On leave from Institut of Physics, Jagiellonian University, Crakow, Poland.

1. - INTRODUCTION

The CdTe-MnTe solid solutions, which combine the semiconducting properties of CdTe with the magnetic properties of $3d^5$ states of Mn, have been recently studied with the main aim of having a consistent explanation of their magnetic and electronic properties. Up to now, many significant results have been reported on this system, concerning the optical[1-4], the magnetooptical[5-7], the transport[8] and the magnetic[9-12] properties throughout a wide range of Mn content. Nevertheless, there are still essential contradictions in conclusions drawn from some investigations. In particular the photoluminescence studies[13] indicate that the d-electrons of Mn are localized and placed about 1 eV below the top of the valence band. On the other hand, the integral[14] and the angle-dependent[15] photoemission studies may suggest a large delocalization and strong hybridization of the Mn 3d levels with the Te 5p valence band.

The atomic scale structure of the zinc-blende-type ternary alloys (like $Cd_{1-x}Mn_xTe$) is still an open question too. CdTe and MnTe crystallize in cubic (zinc-blende) and hexagonal (NiAs) structure, respectively. Standard X-ray diffraction measurements suggest that $Cd_{1-x}Mn_xTe$ crystallizes in zinc-blende structure up to $x = 0.7$ and undergoes a structural phase transition to a multiple-phase system at higher concentration of manganese[16, 17]. The lattice constant of this material changes linearly with x in the whole single-phase region[18], the feature commonly referred to as Vegard's Law. Such behavior does not exclude a bimodal distribution of the nearest-neighbor (NN) distances in the alloy. Diffraction methods do not provide sufficient structural information on the local distances of atoms in crystals. A new insight was recently supplied by the extended X-ray absorption fine structure (EXAFS) analysis applied to the $In_{1-x}Ga_xAs$ alloy by Mikkelsen and Boyce[19] and by Azoulay et al.[20] to the $Er_{1-x}Pr_xSb$ alloy although in a very narrow range of composition x. Those works together with our experimental results reported earlier for $Cd_{1-x}Mn_xTe$[21, 22] yield the conclusion that impurity atoms create a bimodal distribution of the NN distances.

There was other experimental evidence which obliged us to consider the NN and NNN (next-nearest-neighbor) order in this alloy. For instance, the analysis of an anomalous behavior of $Cd_{1-x}Mn_xTe$ fundamental reflectivity spectra measured versus Mn concentration[18, 23, 24] which might suggest the local disorder induced by Mn atoms, or the results of the investigation of the magnetic properties obtained by Galazka et al.[10]. Moreover, the recent calculation of the electronic states in hypothetic, cubic

MnTe[25] in which authors used the lattice constant extrapolated to x = 1 from the linear behavior in the homogeneity region, showed that, regardless on the assumed charge transfer, the resulting structure was metallic, in apparent contradiction with expectations. The improper structural information used there was perhaps a reason for this discrepancy. Therefore definite structural information is apparently needed to explain the electronic and magnetic properties of $Cd_{1-x}Mn_xTe$.

Our paper is just devoted to that problem. In Section 2 we present the results of the EXAFS measurements performed on binary compounds CdTe and MnTe and on their alloys and discuss the NN distances between components. Next, in Section 3, we develop a model of the microscopic structure of the zinc-blende-type $A_{1-x}B_xC$ ternary alloys which explains consistently the experimentally found bimodal distribution of NN distances. Section 4 contains the summary of our experimental and theoretical results, a comment about the different approximations in the theory of alloys and, finally, a discussion about the stability of $Cd_{1-x}Mn_xTe$ alloy.

2. - EXPERIMENTAL DETAILS AND DATA REDUCTION

The EXAFS measurements were performed at the National Radiation Facility "PULS" of Frascati (Italy) with the light emitted by the Adone storage ring (1.5 GeV, 50 mA). The experimental set up is described elsewhere[26].

Single crystals of CdTe and MnTe and of their alloys were powdered and supported on kapton and mylar adhesive tape or deposited from a water dispersion on Millipore membranes. For CdTe thin films 2.6 μm thick evaporated onto a mica substrate were also used. EXAFS spectra were measured at three different temperatures 300, 150 and 80 K for Mn concentrations x = 0, 0.1, 0.3, 0.5, 0.7, 1. The edges considered were the Te L_{III} and L_I, the Cd L_{III} and L_I and Mn K at 4341, 4939, 3537, 4018 and 6543 eV, respectively. The Mn K edge was measured by fluorescence. In MnTe the steepest edge was at 6545 eV. The average resolution was better than 10^{-4} in this energy range. To check the homogeneity of our solid solutions in the whole composition range and to measure their lattice constant, we performed an X-ray diffraction study. In Fig. 1 we present the measured lattice constant as a function of the Mn fraction x. The X-ray results indicated that the alloys were not composed of separate CdTe and MnTe phases and that the average lattice constant varied linearly through the entire solid solution.

The extraction of the EXAFS modulation function $\chi(k)$ from the background was made with the usual procedure of data reduction, i. e., a Victoreen fit to subtract the

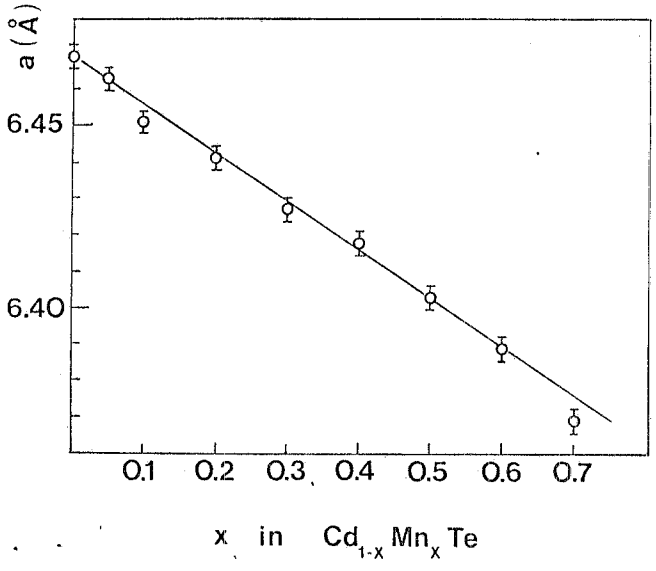

FIG. 1 - The lattice constant of $Cd_{1-x}Mn_xTe$ versus Mn content x as measured by X-ray diffraction.

preedge background followed by a spline line fit to the atomic-like smooth background. This procedure yields the well-known EXAFS function

$$\chi(x) = \sum_j N_j \frac{f_j(\pi, k)}{R_j^2} \exp(-2R_j/\lambda) \exp(-2k^2\sigma_j^2) \sin(2kR_j + \varphi_j(k)), \qquad (1)$$

where N_j is the coordination number of the jth shell at a distances R_j from the absorber, $f_j(\pi, k)$ is the backscattering amplitude for the jth atom, $\varphi_j(k)$ is the total (backscatterer and absorber) phase shift, $\lambda(k)$ is the mean free path of the excited electron and σ_j^2 is the mean square relative displacement of the absorber-scatterer pair. The photoelectron wave-vector k is given by

$$\hbar\omega = E_o + \frac{\hbar^2 k^2}{2m} , \qquad (2)$$

where E_o, the photoabsorption threshold, has been taken to coincide with the maximum of the derivative at the absorption edge.

The total phase and backscattering amplitude for the jth shell were obtained from the usual analysis[27] in k space. Namely, the $k\cdot\chi(k)$ data were Fourier transformed (FT) to real space and the contribution of the single shell j was backtransformed to extract the phase and amplitude functions. From Eq. (1) the total phase factor $\varphi_j(k)$ for a given shell j contained in the sine function can be extracted if the interatomic distance is known, viz., a suitable structural standard can be found. In our case the zinc-blende CdTe and the hexagonal MnTe binary compounds were adopted. Uder the assumption of the phase transferibility for a given absorber-backscatterer pair, i. e.

$\varphi_j^x(k) = \varphi_j^M(k)$, and from the relation $\Phi_j^x(k) = 2kR_j^x + \varphi_j^x(k)$ the interatomic distance $R_j^x(k)$ for the unknown is simply given by

$$R_j^x(k) = (\Phi_j^x(k) - \varphi_j^M(k))/2k \,, \tag{3}$$

where M stands for model compound. Before discussing the ternary alloys data, we shall examine the EXAFS of the standards at their different edges.

2.1. - CdTe

CdTe, similarly to a large number of II-VI compounds, is a semiconductor which crystallizes in the zinc-blende structure. This structure is characterized by the tetrahedral coordination of atoms, i.e., each atom of Cd is surrounded by four NN Te atoms at the same distance. Cd ($Z = 48$) and Te ($Z = 52$) are near in the Periodic Table and this implies that their backscattering functions should be rather similar. For intermediate-Z atoms this function exhibits a double peak due to the Ramsauer-Townsend effect[27]. As a result we expect a double peak in the modulus of F(R), provided $\chi(k)$ is transformed on an extended enough k range.

The Te L_{III}-edge EXAFS of CdTe is presented in Fig. 2 together with its FT calculated in the range $2.6 \leq k \leq 8.1$ Å^{-1} using a Hanning window function. The first peak is double and corresponds to the first Cd shell at $R = 2.80$ Å. The experimentally derived amplitude function $f(\pi, k)$ for this shell is given by

$$f(\pi, k) = \frac{A(k)\, R_{CdTe}^2}{N_{Cd}\, e^{-2R_{CdTe}/\lambda(k)}\, e^{-2k^2\sigma_{CdTe}^2}} \,. \tag{4}$$

The amplitude function $f(\pi, k)$, is plotted in Fig. 2c and displays a clear double maximum. The comparison with the theoretical amplitude function from Teo and Lee tabulations[28] indicates that only rough agreement exists. Considerable work has been done on ZnSe and ZnTe by Stern et al.[29] who based their analysis of the EXAFS spectra on the influence of many-body effects on the amplitude backscattering function. Fitting the spectra with the theoretical parameters and correcting for the electron-electron interaction through external S_o^2 and λ parameters, reasonable agreement with the experiment was achieved. On the other hand, Pettifer[30] critically examined the EXAFS results for ZnSe and ZnTe and concluded that the agreement between theory and experiment was not satisfactory for shells other than the first. The main difficulty was found in the use of the plane-wave approximation for the backscattering functions. The

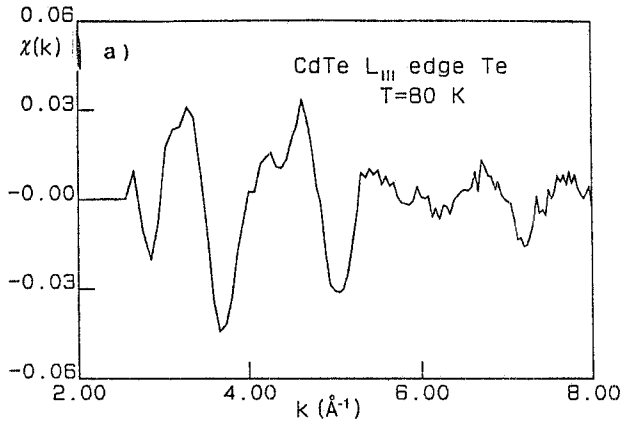

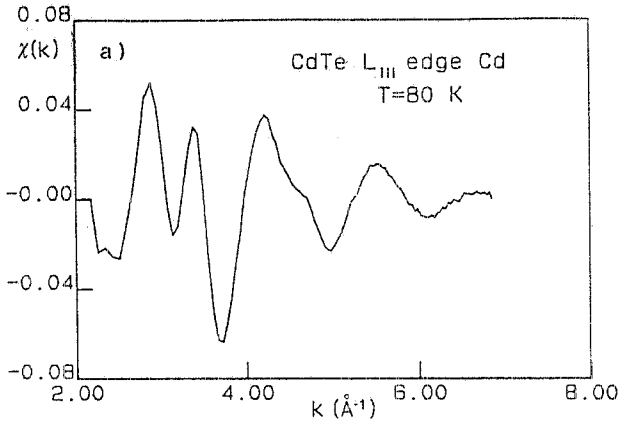

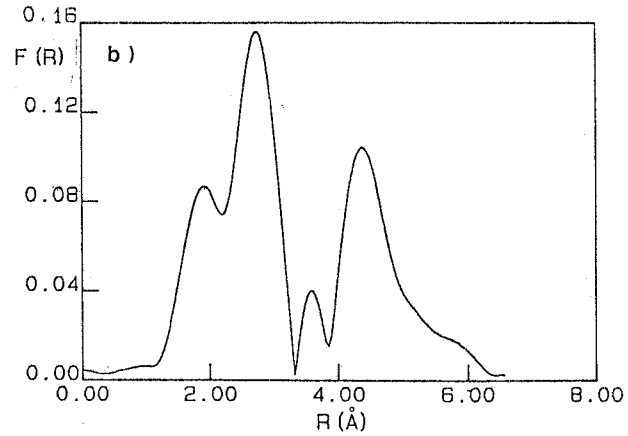

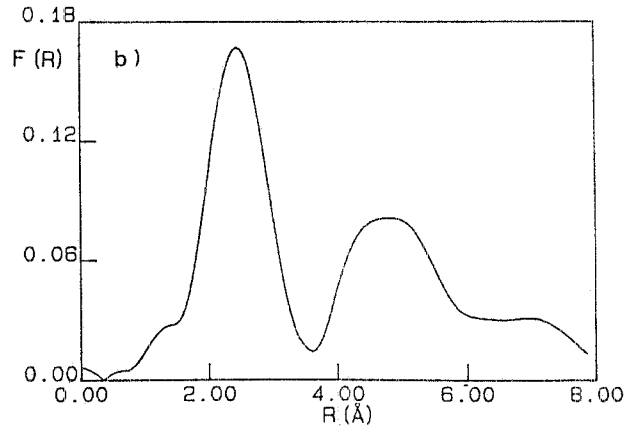

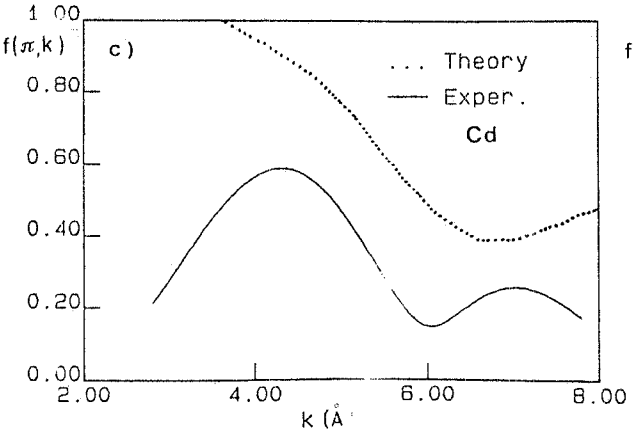

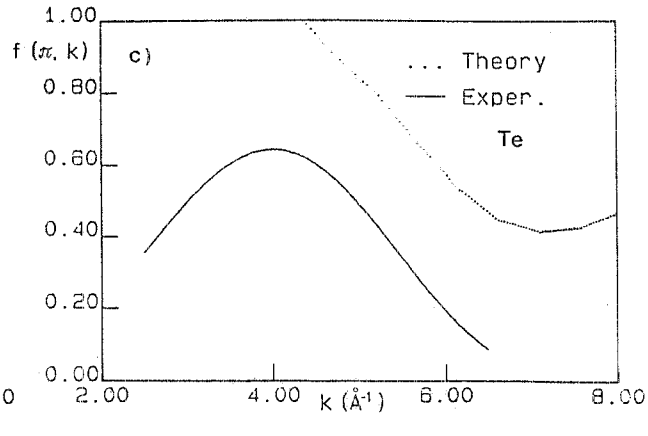

FIG. 2 - a) EXAFS modulation function $\chi(k)$ above the L_{III} edge of Te in CdTe; b) Modulus F(R) of the FT of $\chi(k)$ in the range 2.6 k 8.1 $Å^{-1}$ using a Hamming window function; c) comparison between the theoretical (dotted line) and the experimental amplitude functions of Cd obtained by backtransforming the first two peaks of F(R).

FIG. 3 - a) EXAFS modulation function $\chi(k)$ above the L_{III} edge of Cd in CdTe; b) Modulus F(R) of the FT of $\chi(k)$ in the range $2.0 \leq k \leq 6.7$ $Å^{-1}$ using a Hanning window function; c) comparison between the theoretical (dotted line) and the experimental amplitude functions of Te obtained by backtransforming the first peak of F(R).

se functions differ strongly for heavier elements ($Z > 40$) at values of k lower than 8 $\mathring{A}^{-1}$ from those calculated within the spherical wave approximation. In distinction to Stern et al.[29], Pettifer[30] suggests a significant effect on the NN backscattering of the curvature of the outgoing electron wave for all chalcogenides zinc compounds ZnS, ZnSe, ZnTe.

A preliminary analysis of CdTe was made on the same lines of a previous study[21] where the main interest was on the corrections to be applied to Eq. (1). At the L_{III}-edge of Cd, measured at 80 K, the NN Te shell is not resolved into two structures like at the Te L_{III}-edge because of the narrower range of k accessible to the measurements (Fig. 3). Furthermore the amplitude function in Fig. 3c shows that the second peak occurs at values of k larger than 6 $\mathring{A}^{-1}$. Although the identification of the main features of F(R) can generally be made using only theoretical scattering functions[21], the exact knowledge of these functions is hardly achievable. In view of these difficulties we treat CdTe as a standard from which these functions are experimentally derived and used in the analysis of the alloys.

2. 2. - MnTe

MnTe has a well-defined hexagonal crystallographic structure (NiAs-type lattice) in which Mn is sixfold coordinated to Te with a NN distance of 2.909 $\mathring{A}$. Here we are interested to achieve experimental scattering functions for the Mn-Te and the Te-Mn pairs to build a model environment for the cubic $Cd_{1-x}Mn_xTe$ alloys, by using the concept of transferability of the scattering phase in the high electron kinetic energy regime. We have measured therefore the EXAFS structure above the Mn K-edge and the Te L_{III}-edge in MnTe which are shown in Fig. 4a and Fig. 5a, respectively. The corresponding F(R) are displayed in Fig. 4b and Fig. 5b, respectively. In Fig. 4c and Fig. 5c we present the $f_j^M(\pi, k)$ function extracted using the same procedure as described above. These functions are used subsequently to fit the $Cd_{1-x}Mn_xTe$ EXAFS data.

2. 3. - $Cd_{1-x}Mn_xTe$

2. 3. 1. - Cd L_{III}-edge

The F(R) spectra around the Cd L_{III}-edge for $x = 0.1$, 0.3, 0.5 and 0.7 in $Cd_{1-x}Mn_xTe$ are illustrated in Fig. 6. Due to the limited k range accessible above this edge free from the absorption of the L_{II} Cd edge, the achieved resolution in the r spa

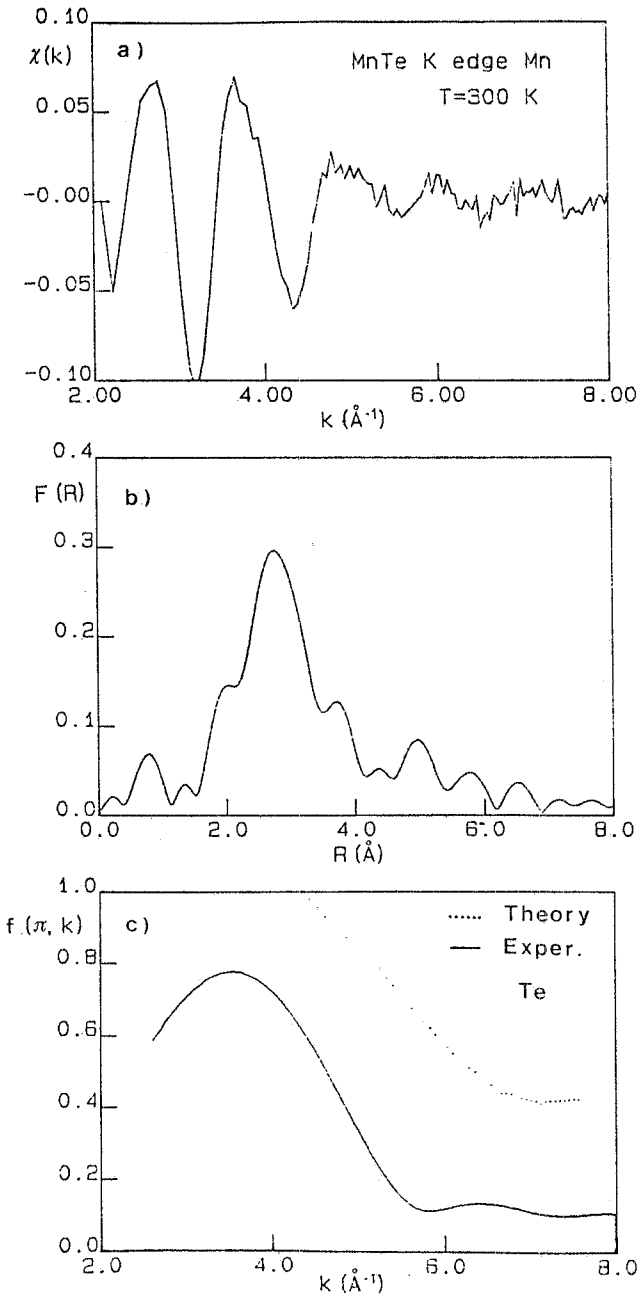

FIG. 4 - a) EXAFS modulation function $\chi(k)$ above the K edge of Mn in MnTe; b) Modulus F(R) of the FT of $\chi(k)$ in the range $2.1 \leq k \leq 8.5$ Å^{-1} using a Hanning window function; c) comparison between the theoretical (dotted line) and the experimental amplitude functions of Te obtained by backtransforming the peak of F(R) between 1.5 and 3.4 Å.

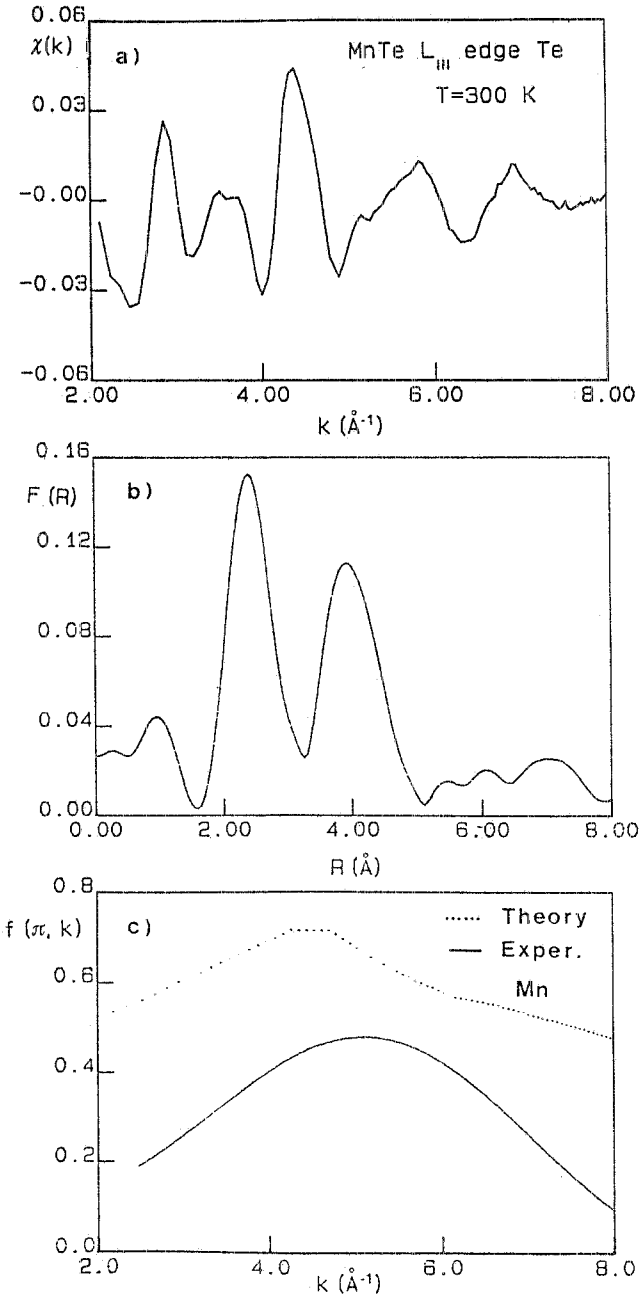

FIG. 5 - EXAFS modulation function $\chi(k)$ above the L_{III} edge of Te in MnTe; b) Modulus F(R) of the FT of $\chi(k)$ in the range $2.1 \leq k \leq 8.5$ Å^{-1} using a Hanning window function; c) comparison between the theoretical (dotted line) and the experimental amplitude functions of Mn obtained by backtransforming the first peak of F(R).

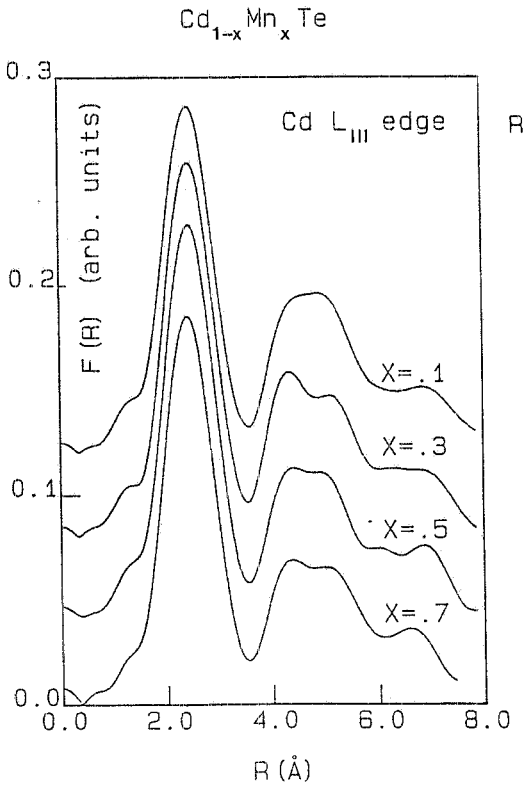

FIG. 6 - Modulus F(R) of the FT of $\chi(k)$ measured above the Cd L_{III} edge in $Cd_{1-x}Mn_xTe$ for several concentrations x.

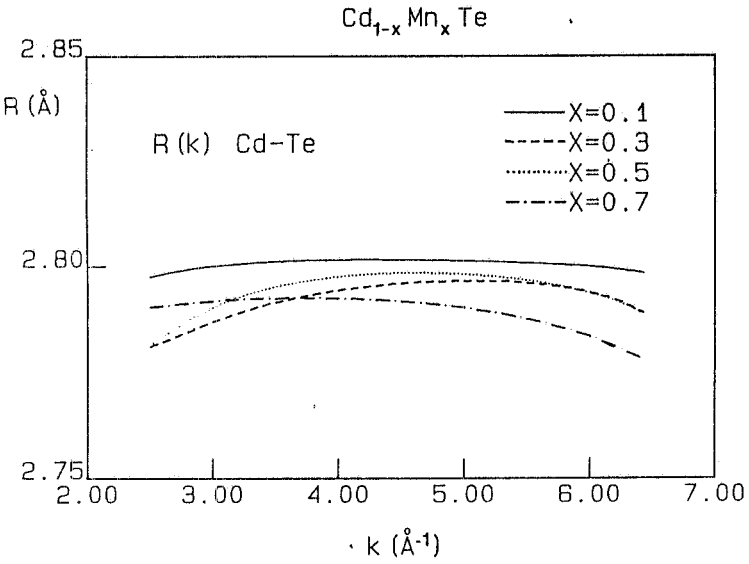

FIG. 7 - Nearest-neighbor Cd-Te distances versus k as derived from the EXAFS analysis of $Cd_{1-x}Mn_xTe$ for several concentrations x.

ce is worse than around Te and the double components of the first peak are not observed. Moreover, the width of the Te peak is approximately the same for the various concentrations of manganese. By filtering out the first peak of F(R) and backtransforming it in the range $1.5 \leq R \leq 3.5$ Å we obtained from Eq. (3) the R(k) values of the Cd-Te pair for various x, which are shown in Fig. 7. Within the estimated error bar for this distance ($\pm$ 0.01 Å), we measured a Cd-Te distance as equal to 2.80 Å for all concentrations. Such a distance is coincident with that of pure CdTe.

2.3.2. - Mn K-edge

The above analysis applied to the Mn K-edge yields a distance of the Te-Mn pair ranging from 2.76 ± 0.01 Å for $x = 0.1$ to 2.74 ± 0.01 Å for $x = 0.7$. The measured F(R) spectra are shown in Fig. 8 and the R(k) function is plotted in Fig. 9 for various x.

2.3.3. - Te L_{III}-edge

Fig. 10 shows the F(R) function above the Te L_{III}-edge for x increasing from 0.1

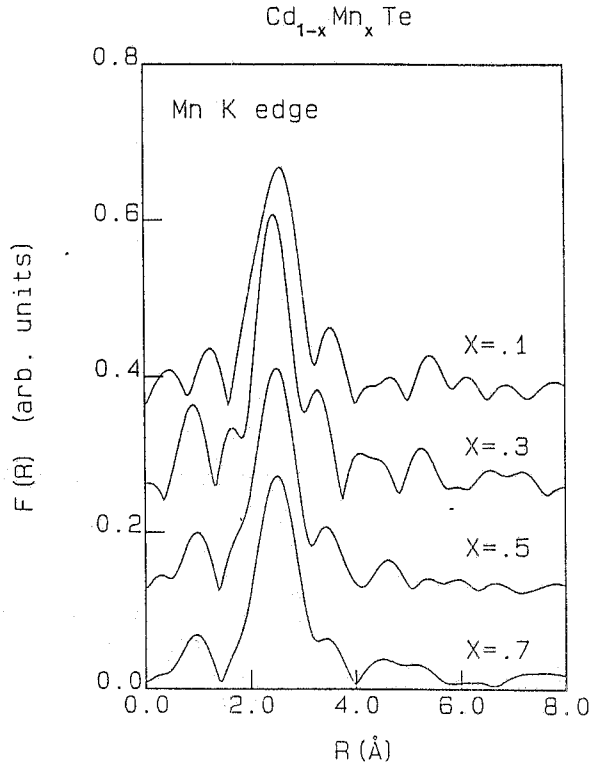

FIG. 8 - Modulus F(R) of the $\chi(x)$ measured above the Mn K edge in $Cd_{1-x}Mn_xTe$ for several concentrations x.

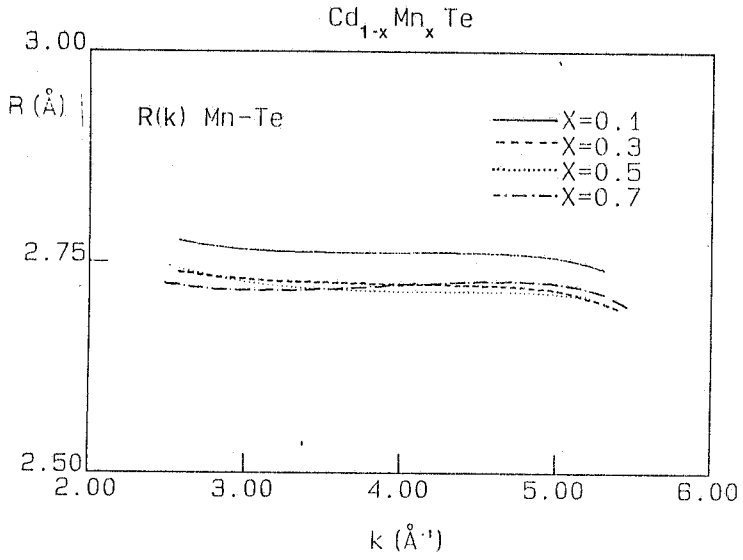

FIG. 9 - Nearest-neighbor Mn-Te distances versus k as derived from the EXAFS analysis of $Cd_{1-x}Mn_xTe$ for several concentrations x.

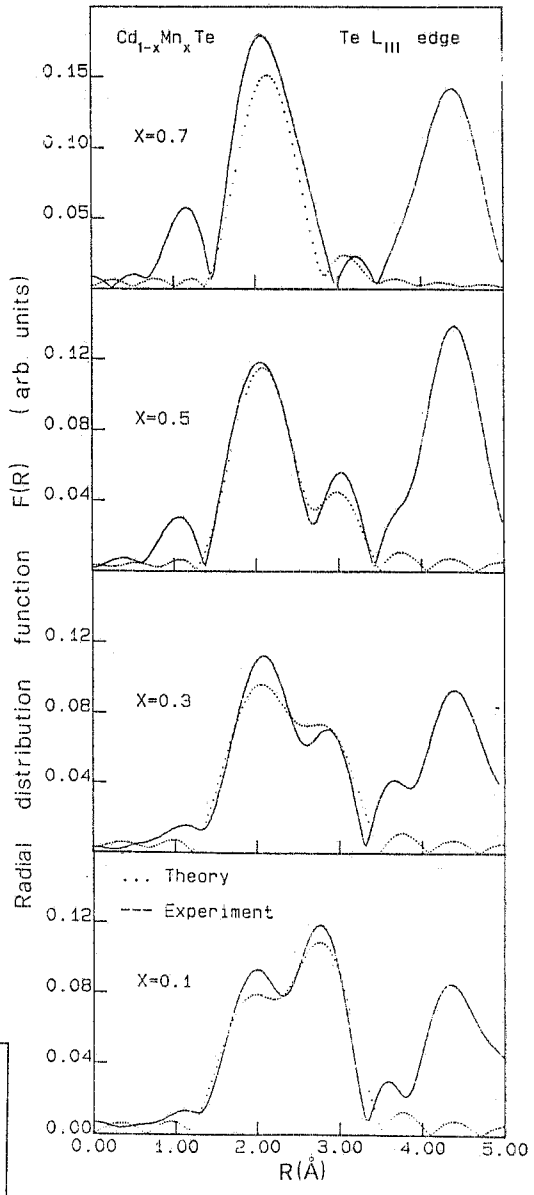

FIG. 10 - Modulus F(R) of the FT of $\chi(x)$ at the L_{III} edge for four Mn concentrations x in $Cd_{1-x}Mn_xTe$ (full lines). The dotted lines are the best-fit curves for the nearest-neighbor Mn and Cd atoms surrounding Te.

to 0.7, calculated in the range $2.6 \leq k \leq 8.1$ Å. The first and second peaks of F(R) correspond to the NN Mn and Cd atoms, respectively, in the first shell aurrounding Te. By increasing the mole fraction of Mn the intensity of the Mn peak increases and, correspondingly, the intensity of the Cd peak decreases. As discussed in the case of pure CdTe, the Cd peak is double and thus the Mn peak in the alloy is superimposed on the lateral peak of Cd.

We have best fitted F(R) by using as free parameters the anion-cation distances and the Debye-Waller factors for Mn and Cd atoms (Table I). The starting values were

TABLE I - The best-fit anion-cation distances R, Debye-Waller factors σ^2 and change of E_o for the Mn-Te and CdTe pairs.

	Mn - Te			Cd - Te		
x	R(Å)	σ^2 (x10^{-2} Å^2)	E_o(eV)	R(Å)	σ^2 (x10^{-2} Å^2)	E_o(eV)
0.1	2.755	0.01	0.311	2.801	0.60	0.068
0.3	2.748	0.01	0.309	2.801	0.78	0.357
0.5	2.747	0.25	0.370	2.800	0.65	2.57
0.7	2.74	0.20	0.584	2.795	0.50	4.99

those derived from the analysis of the Cd L_{III} and Mn K-edges in $Cd_{1-x}Mn_xTe$. The amplitude and phase functions were determined from the model compounds and the coordination numbers were calculated from the nominal x in the alloy. The best fit F(R) curves are reproduced in Fig. 10 (dotted lines) for various x and agree satisfactorily with the experimental curves. The anion-cation distances are almost independent of x and are shown in Fig. 11 (full dots). In $In_{1-x}Ga_xAs$ Mikkelsen and Boyce[19] cannot directly observe the splitting of the cation peak but they observe a broadening and a small shift of the NN peak compared with pure binary compounds. They resolve it by a fitting procedure using two Gaussian distributions.

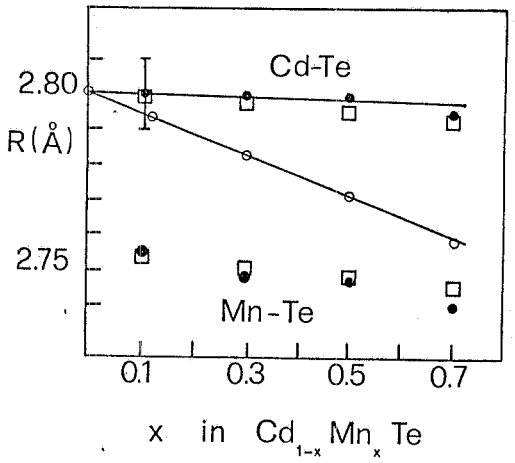

FIG. 11 - The average Cd-Te and Mn-Te nearest-neighbor distances in $Cd_{1-x}Mn_xTe$ alloys versus concentration x. • Values from the best-fit of the EXAFS data; □ Values calculated from the model; o Values of a(x) /3/4, as measured by X-ray diffraction.

In $Cd_{1-x}Mn_xTe$ the further peaks of F(R) between 3 Å and 5 Å are assigned to NNN Te and Cd (Mn) atomic shells. The intensity of this complex structure grows with increasing x.

3. - THE MODEL OF THE MICROSCOPIC STRUCTURE OF RANDOM ALLOYS

Taking into account all the experimental evidence, it seems that a general property of random solid solutions of binary compounds has been discovered: the A-C and B-C distances in the zinc-blende-type $A_{1-x}B_xC$ alloy at arbitrary concentration are nearly the same as in pure AC and BC compounds, respectively. It is, therefore, very interesting to consider in detail how the zinc-blende structure accomodates two different cation-anion distances. Mikkelsen and Boyce[19] drew an analogy between $A_{0.5}B_{0.5}C$ alloy and chalcopyrite (ABX_2) crystallographic structures. Following their approach directly one cannot, however, describe an alloy at arbitrary concentration x.

In order to develop a model possessing such a capability one must realize that NN distances, as measured by EXAFS, are an average over a macroscopic volume. It implies that a model must be statistical, and proper averaging over possible NN distances should reproduce the experimental data.

To start with, we shall consider which sublattice is more likely to be distorted. Our measurements do not provide enough information to analyse the NN distances. Mikkelsen and Boyce[19] report that the cation-cation distribution has a single peak and it is only slightly broadened comparing to that in the pure compound, whereas the anion-anion distribution is bimodal. Such experimental evidence suggest that much stronger distortion occurs to the anion sublattice. Moreover, as Mikkelsen and Boyce pointed out, if the cation sublattice were to distort, the average anion-cation distance could not differ much from the virtual-crystal approximation (VCA) value. Decreasing the distance of a cation from some anion we increase the other cation-anion distances in the same tetrahedron, keeping the average close to the VCA value. Finally, we point out that if we believe that the NN interactions are dominant in the alloy, it is much more likely that the anion surrounded by different cations will leave its central position in the tetrahedron instead that the same would happen to the cation surrounded always by four identical anions. The assumption about the dominant role of NN interactions is made in the majority of alloy models.

3.1. - Formulation of the model

Taking into account the above considerations we construct our model of the microscopic structure of the zinc-blende-type $A_{1-x}B_xC$ alloy according to the following:

a) We assume that the cation sublattice remains undirstorted (In general, the sublattice containing two types of atoms remains undirstorted).

b) We consider all possible coordinations around an anion in the alloy - there can be 0, 1, 2, 3 and 4 B-type cations at the vertices of the tetrahedron. For every coordination we consider the relationship between A-C and B-C distances when an anion is displaced from its central position. We assume that the influence of disorder in the NNN and further shells does not affect a displacement of a central anion. The NNN interactions are much smaller than NN ones but it is not necessary to assume that they are negligible. It is enough to observe that, due to the long-range disorder, the net displacing force acting on a central anion will be close to zero. Fig. 12 shows all possible geometrical situations for the 3 cases in which we have 1, 2 or 3 B-type cations in a tetrahedron. We assume that the anion has a ten

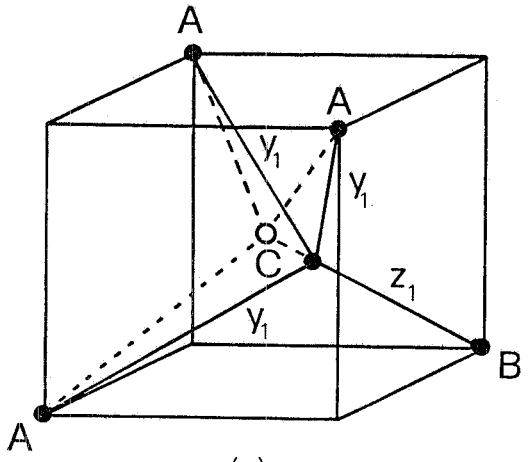

(a)

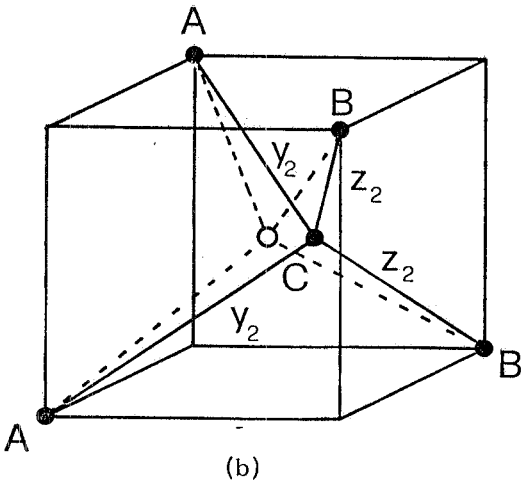

(b)

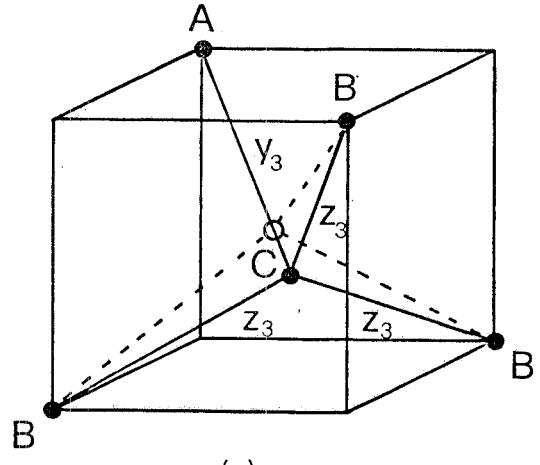

(c)

FIG. 12 - All possible coordinations around the anion in the tetrahedra containing both types of cations. The open point and dashed lines mark the positions of the central anion and the bonds in tetrahedra when the anion sublattice is undirstorted. The solid lines and full points mark the bonds and the positions of ion in distorted tetrahedra.

dency to get closer to the B-type cation (in our case B-type cation is Mn, in Mikkelsen and Boyce's case[19] it is Ga).

If $z_n(x)$ denotes the B-C distances, the A-C distances are given by

$$y_1(x) = \sqrt{\frac{a^2(x)}{2} + z_1^2(x) - \frac{2a(x)}{\sqrt{3}}\, z_1(x)}\,,$$

$$y_2(x) = \sqrt{\frac{a^2(x)}{4} - a(x)\sqrt{z_2^2(x) - \frac{a^2(x)}{8}} + z_2^2(x)}\,, \qquad (5)$$

$$y_3(x) = \frac{a(x)}{\sqrt{3}} - \frac{1}{2}\sqrt{4z_3^2(x) - \frac{2}{3}a^2(x)}\,,$$

for the cases a, b and c in Fig. 12, respectively; a(x) denotes the lattice constant of the alloy at concentration x. In the case when all four cations are the same, the tetrahedron cannot be distorted - the B-C (or the A-C) distance equals $y_o = z_4 = a(x)\sqrt{3}/4$.

c) For the next step we must consider the probability of finding tetrahedra with 0, 1, 2, 3 and 4 B-type cations in the alloy at concentration x. Let us consider an anion picked up at random distribution of cations in their sublattice. Obviously, the probability of finding the B-type cation at any vertex of the tetrahedron is equal to x and the probability of finding the A-type cation is 1-x. Hence, the probability of finding a tetrahedron with n B-type cations is given by the binomial Bernoulli distribution:

$$P(n,x) = \binom{4}{n} x^n (1-x)^{4-n} \qquad (n = 0, 1, 2, 3, 4)\,. \qquad (6)$$

Some remarks, concerning Mikkelsen and Boyce's model[19] are in order here. They claimed that in $A_{0.5}B_{0.5}C$ alloy the tetrahedra containing 1 and 3 and 3 and 1 A-type and B-type cations, respectively, should occur 4.2 times less frequently than those with 2A and 2B cations. Their analogy to chalcopyrite is based on the observation that in the $A_{0.5}B_{0.5}C$ alloy tetrahedra with 2A and 2B cations were predominant. This is, unfortunately, not the case because in accordance to formula (6) for x = 0.5 the probability of finding a tetrahedron with 2A and 2B cations is 3/8 whereas of 1-3 and 3-1 configurations are 1/4. Hence, it is more likely that we will find a tetrahedron with 1-3 or 3-1 than with 2-2 configuration even for x = 0.5. It makes the validity of their chalcopyrite analogy questionable[31].

d) Having defined the geometry and the probability distribution of different possible tetrahedra one can calculate the average NN distances. It can be done if distances $y_n(x)$

and $z_n(x)$ are properly weighted by probabilities (6) and additional weights $W(n) = 4-n$ (and $W(4-n)$) arising from the fact that in the tetrahedron containing n B-type cations there are 4-n A-C (and n B-C) distances. Then, the average A-C and B-C distances denoted by $\bar{y}$ and $\bar{z}$, respectively, are given by:

$$\bar{y}(x) = \frac{1}{P(x)} \sum_{n=0}^{4} W(n)\, P(n,x)\, y_n(x) , \tag{7}$$

where

$$P(x) = \sum_{n=0}^{4} W(n)\, P(n,x) ,$$

and

$$\bar{z}(x) = \frac{1}{P'(x)} \sum_{n=0}^{4} W(4-n)\, P(n,x)\, z_n(x) , \tag{8}$$

where

$$P'(x) = \sum_{n=0}^{4} W(4-n)\, P(n,x) .$$

e) To complete the calculation of the average NN distances we have to know all six values $y_n(x)$, $z_n(x)$ $(n = 1, 2, 3)$ and to realize this, the following procedure is proposed. The $\eta_n(x)$, given below, are minimized as the functions of $z_n(x)$ for all cases $n = 1, 2, 3$ and for each value of x

$$\eta_n(x) = \frac{3\alpha_z}{8z_p^2} W(4-n)\,(z_n^2(x) - z_p^2)^2 + \frac{3\alpha_y}{8y_p^2} W(n)\,(y_n^2(x) - y_p^2)^2 . \tag{9}$$

The z_p and y_p denote the B-C and A-C NN distances in the pure BC and AC compounds, and α_z and α_y denote the bond-stretching constants of these compounds, respectively. The functions (9) can be interpreted as the energies which are needed for changing the length of bonds and they are written on the basis of Keating's[32] scheme of the valence-force-field (VFF) approach[33]. The bond-stretching constants are taken from the paper of Martin[34]. Furthermore, it should be noticed that the proposed minimization procedure follows the empirical observation mentioned already above, that the A-C and B-C NN distances in the $A_{1-x}B_xC$ alloy tend to be, as far as possible, the same as in the pure compounds. That the minimization is carried out for each configuration of atoms in each tetrahedron is consistent with the assumption of the predominant role of the NN interactions.

The procedure used in our model can be summarized in a few words:

- the set of values $z_n(x)$ and $y_n(x)$ has been obtained by means of the minimization of

functions (9) with the use of relations (5);
- from Eq. (7) and Eq. (8) $\bar{z}(x)$ and $\bar{y}(x)$ - the average NN distances - were calculated.

The sufficient input data for the calculation are the lattice constants of the alloy a(x) and the bond-stretching constants of the components. Obviously, $z_p = a(1)\sqrt{3}/4$ and $y_p = a(0)\sqrt{3}/4$.

3. 2. - Application to $Cd_{1-x}Mn_xTe$ and $In_{1-x}Ga_xAs$ alloys

The lattice constants for CdTe ($a(0) = 6.468$ Å) and $Cd_{1-x}Mn_xTe$ ($0 \leq x \leq 0.7$) were obtained from the X-ray diffraction data[18]. The linear dependence of a(x) was extrapolated and the value $a(1) = 6.333$ Å for pure MnTe was obtained. The bond-stretching constants, as mentioned above, were taken from the paper[34]. For CdTe, $\alpha_{CdTe} = 29.02$ and for the MnTe the value $\alpha_{ZnTe} = 31.35$ was used as an approximation. The Zn atom differs from the Mn atom by five d electrons (Zn: $3d^{10}4s^2$, Mn: $3d^5 4s^2$) but they have the same number of valence electrons. Hence, we believe that the stretching constant for the Zn-Te bond does not differ much from the MnTe one.

The results of calculations for $Cd_{1-x}Mn_xTe$ are illustrated in Fig. 11 and detailed values are presented in Table II. Fig. 13 and Table III show the results of the application of our model to Mikkelsen and Boyce's data[19]. The bond-stretching constants of InAs and GaAs were also taken from the paper[34]. In both cases the agreement is very good.

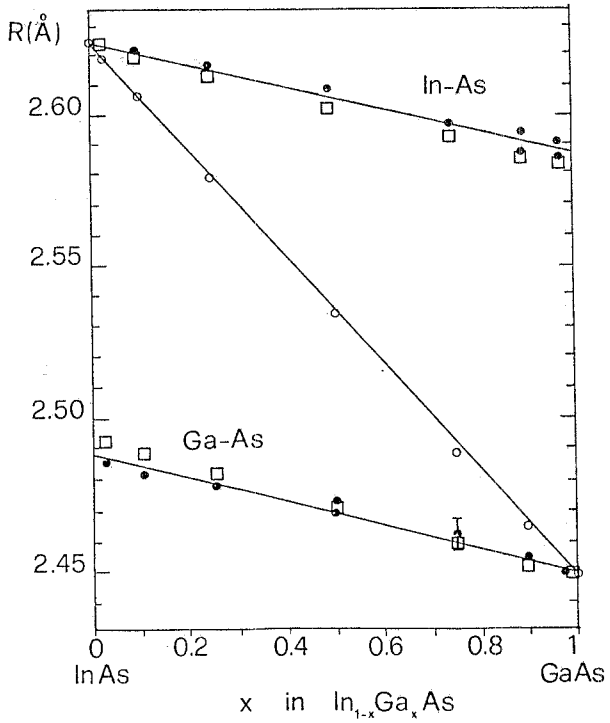

FIG. 13 - The average In-As and Ga-As nearest-neighbor distances in $In_{1-x}Ga_xAs$ alloy versus concentration x. All marks are the same as in Fig. 11.

3. 3. - Additional comments on the model

Finally, we would like to add the following remarks:

a) Further improvement of the model is possible by including the bond-bending terms into functions (9). In this way the full Keating's scheme[32] will be employed.

b) In some further applications not only the average values $\bar{z}$ and $\bar{y}$ but the detailed distances z_n and y_n (as listed in

Table II and Table III) may be useful as well.

TABLE II - The NN distances in $Cd_{1-x}Mn_xTe$ alloys versus concentration x. The values y_1, y_2, y_3 and z_1, z_2, z_3 are the distances obtained for different configurations a, b and c in Fig. 12, respectively. $\bar{y}$ and $\bar{z}$ are the NN average distances. a(x) is the lattice constant and $a(x)\sqrt{3}/4$ is the NN distance in the undistorted tetrahedron. All distances are in Å.

x	a(x)	Cd - Te distance				$\frac{a(x)\sqrt{3}}{4}$	Mn - Te distances			
		$\bar{y}$	y_1	y_2	y_3		z_1	z_2	z_3	$\bar{z}$
0.1	6.455	2.800	2.810	2.826	2.841	2.795	2.751	2.765	2.780	2.755
0.3	6.428	2.797	2.798	2.813	2.829	2.783	2.740	2.754	2.768	2.752
0.5	6.407	2.794	2.786	2.801	2.817	2.772	2.728	2.743	2.757	2.750
0.7	6.374	2.791	2.774	2.789	2.804	2.760	2.717	2.731	2.745	2.747

TABLE III - The NN distances in $In_{1-x}Ga_xAs$ alloys versus concentration x. All symbols are the same as in Table II.

x	a(x)	In-As distance				$\frac{a(x)\sqrt{3}}{4}$	Ga-As distance			
		$\bar{y}$	y_1	y_2	y_3		z_1	z_2	z_3	$\bar{z}$
0.025	6.048	2.622	2.666	2.715	2.765	2.619	2.486	2.529	2.574	2.489
0.1	6.016	2.619	2.652	2.701	2.749	2.605	2.473	2.516	2.560	2.486
0.25	5.954	2.613	2.624	2.672	2.720	2.578	2.450	2.491	2.534	2.481
0.5	5.852	2.601	2.577	2.624	2.671	2.534	2.411	2.450	2.492	2.471
0.75	5.753	2.589	2.533	2.577	2.624	2.491	2.374	2.410	2.450	2.461
0.9	5.690	2.580	2.504	2.548	2.594	2.464	2.350	2.385	2.424	2.452
0.99	5.660	2.577	2.490	2.533	2.579	2.451	2.339	2.373	2.411	2.450

c) A general structure of the model is that the average positions of the anions in the distorted sublattice (Te in our case and As in Mikkelsen and Boyce's case[19]) over all possible 15 different positions is at the center of the tetrahedron (The existence of 15 different positions in distorted sublattice can be immediately seen as follows: in an undirstorted tetrahedron the anion is always in the center; for the configurations a, b and

c shown in Fig. 12 there are 4, 6 and 4 equivalent positions, respectively). This means that the average over all possible NNN distances between anions will not differ from the value of the NNN distance in an undirstorted sublattice, or, in other words, from the VCA value. In spite of that, the distribution of the NNN distances between anions will show the bimodal character similar to that for the NN distances. All particular NNN anion distances be split into two groups. The distances C-A-C and C-B-C will group close to those values in the pure AC and BC compounds, respectively. This qualitative description will be supported by a detailed calculation being in progress. Such a behavior of the NNN distances has been found experimentally in $In_{1-x}Ga_xAs$ alloys[19].

d) Our model, in fact does not consider the problem of the violation of the random distribution of cations in the alloy. All quantitative results and conclusions drawn from it when confronted with experimental data of different measurements (X-ray diffraction, EXAFS, magnetic) may or not confirm such a violation.
However, there is an explicit evidence that for the diluted $In_{1-x}Ga_xAs$ alloy the distribution of the cations is random and the deviation from randomness is estimated to be not larger than 15% for concentrated alloys[19]. Investigations of the magnetic properties of $Cd_{1-x}Mn_xTe$ by Gałązka et al.[10] support basically a statistical distribution of Mn ions[35]. Further support against chemical clustering of Mn ions may be drawn from EXAFS studies of other magnetic alloys[36]. Nevertheless, we are considering the possibility - or necessity - of taking into account, on the top of the present version of the model, a correlation between different tetrahedra.

e) The expression for the average over all NN distances can be written in two equivalent forms (see Eq. (7) and Eq. (8))

$$D = \frac{1}{P(x)+P'(x)}\left[\sum_{n=0}^{4} W(n)\,P(n,x)\,y_n(x) + \sum_{n=0}^{4} W(4-n)\,P'(n,x)\,z_n(x)\right] , \qquad (10)$$

or

$$D = (1-x)\,\bar{y}(x) + x\,\bar{z}(x) . \qquad (11)$$

The latter one was proposed by Mikkelsen and Boyce[19]. Comparing Eq. (11) with Eq. (10) one can thus understand the internal structure of the phenomenological expression (11). If we evaluate the expression (10) using all NN distances as listed in Table II and Table III, we will obtain the average NN distance D as measured by X-ray diffraction in the particular cases. Such a test of consistency was done, showing perfect agreement.

f) It is also possible to relax the first assumption of our model and let cations move

a little from the vertices of the tetrahedron. Then the displacements of the ions in both sublattices should be calculated in self-consistent way. Unfortunately, the last idea will change our simple model to a very complex one.

4. - DISCUSSION AND CONCLUSIONS

The EXAFS studies of Te, Cd and Mn edges in $Cd_{1-x}Mn_xTe$ alloy bring the following significant conclusions:

a) At the L_{III} edge of Te (Fig. 10), the NN peak is split into two peaks. The simulation confirms that they are related to Mn and Cd backscatterers at two different distances 2.74-2.755 Å (depending on x) and 2.80 Å from the Te absorber, respectively. In $Cd_{1-x}Mn_xTe$ the modulus F(R) of separated Cd and Mn peaks significantly decreases and increases with the grow of Mn content, respectively.

b) In CdTe at the L_{III} edge of Te, the peak at about 4.3 Å is composed of unresolved peaks due to the Te second shell and the third shell of Cd. In the $Cd_{1-x}Mn_xTe$ alloy the positions of this complex peak does not change appreciably with x.

c) Within the experimental resolution the position and the width of the Te peaks at the Cd L_{III} edge are approximately the same for the various concentrations of Mn. As described in Section 2.3, the Te-Cd average distance equals 2.80 ± 0.01 Å and it is almost independent of x.

d) From the Mn K-edge data, the Te-Mn average distance changes from 2.76 Å to 2.74 Å with increasing x. Also the overall width of the Te peak is approximately the same for various concentrations of Mn.

We would like to emphasize that the NN distances obtained from Cd L_{III} and Mn K edges are in agreement with those obtained from the Te L_{III} edge. These results are direct experimental evidence which confirms the bimodal distribution of the NN distances in $Cd_{1-x}Mn_xTe$ alloy, i.e., ascertains the existence of two different well-defined average distances between Te-Cd and Te-Mn.

The model of the microscopic structure of the zinc-blende-type $A_{1-x}B_xC$ alloys gives all the particular NN distances as well as the average NN distances in very good quantitative agreement with both Mikkelsen and Boyce's[19] and our experimental data. The analysis of the model enables us also to understand qualitatively - detailed calculations are in progress - a behavior of the NNN distances as described in Ref. (19) (our experimental resolution was unsufficient to observe such a subtle changes in $Cd_{1-x}Mn_xTe$).

We believe that the local distortion in zinc-blende-like $A_{1-x}B_xC$ alloys described by our model is a universal feature of such alloys. One of the important consequences is that it makes "classical" definition of the VCA questionable. One either must accept that the VCA is more rough than one has though about and that in this approximation all distortions of the sublattices of the alloys are ignored or one must consider the generalization of the VCA which includes also the proper averaging of the potential of C atoms over all possible position in their distorted sublattice.

The same can be applied to more sophisticated one-electron alloy theories like CPA or ATA. Besides taking into account the scattering on the different cations, one should incorporate into these theories in some way also the effects of averaging the anion potential over different geometrical sites.

Finally, we would like to discuss the problem of the stability of the tetrahedral coordination in $Cd_{1-x}Mn_xTe$ alloy. According to Phillips and Van Vechten approach[37], the ionicity of CdTe is equal to 0.717 which is near to the critical ionicity value (0.785) at which the transition from a covalent to ionic structure or, in other words, the transition from the fourfold (zinc-blende, wurtzite) to the sixfold (rocksalt, NiAs) coordination occurs. Since Mn in MnTe has sixfold coordination, MnTe is reported to be more ionic than CdTe[38]. This indication is supported by core-level shifts from X-ray photoemission spectra[39] and effective charge calculations[40]. The addition of Mn in CdTe should increase the ionicity of bonds in the alloy. The question arises how the crystal structure of $Cd_{1-x}Mn_xTe$ is still cubic up to $x = 0.7$, taking into account that CdTe is just near to the structural phase transition. The answer is that the local distortions of the lattice (distortions of the tetrahedra) described by our model, stabilize the zinc-blende-type structure up to $x = 0.7$. To understand this one should notice the following:

a) In nearly covalent compounds the center of gravity of the bonding charge is placed almost at the middle of the bond, and its shifts towards an anion when the bond ionicity increases.

b) The distortion of the tetrahedra containing 1, 2 or 3 Mn ions, i. e. the shift of Te ions towards Mn, compensate for the displacement of the center of gravity of the bonding charge and decreases the effective bond ionicity. Such a shift is also favored by the smaller ionic radius of Mn^{2+} ions as compared to that of Cd^{2+}.

c) The probability of finding a tetrahedron with 4 Mn ions increases rapidly for $x > 0.7$ (see Formula (6)). Such tetrahedra accordingly to our model cannot distort and the displacement of the bonding charge cannot be compensated. Therefore, the fourfold coordination of $Cd_{1-x}Mn_xTe$ becomes unstable and the transition to the phase typical for ionic compounds occurs.

Summarizing the discussions about the stability of the $Cd_{1-x}Mn_xTe$ alloy we would like to say that phenomenological considerations about the ionicity, supported by conclusions drawn from our theoretical model of the microscopic structure of the alloy, gives a satisfactory, qualitative explanation of this problem.

ACKNOWLEDGEMENTS

We would to thank Prof. W. Giriat, Doc. S. A. Ignatowicz and Dr. K. Weiers for the supply of the samples. We thank also Dr. J. Soltys for his help with X-ray diffraction analysis. The Polish Authors acknowledge the Univesity of Rome II for the financial support and PULS group for the hospitality. One of them (M. P.) wishes also to acknowledge the financial support of Alexander Von Humboldt-Stiftung. The work has been supported in part by the Italian GNSM through the Ministero della Pubblica Istruzione.

REFERENCES

(1) - N. T. Khoi and J. A. Gaj, Phys. Stat. Sol. B83, K133 (1977).

(2) - J. Stankiewicz, N. Bottka and W. Giriat, Proceedings of the 15th Intern. Conf. on the Physics of Semiconductors, Kyoto, J. Phys. Soc. Jap. Suppl. A49, 827 (1980).

(3) - R. A. Abreu, W. Giriat and M. P. Vecchi, Phys. Letters 85A, 399 (1981).

(4) - J. Diouri, J. P. Lascaray and R. Triboulet, Sol. State Comm. 42, 231 (1982).

(5) - J. A. Gaj, R. R. Gałazka and M. Narwrocki, Sol. State Comm. 25, 193 (1978).

(6) - J. A. Gaj, J. Ginter and R. R. Gałazka, Phys. Stat. Sol. B89, 655 (1978).

(7) - G. Rebmann, C. Rigaux, G. Bastard, M. Menant, R. Triboulet and W. Giriat, 16th Intern. Conf. on the Physics of Semiconductors, Montpellier 1982.

(8) - J. Stankiewicz and A. Aray, J. Appl. Phys. 53, 3117 (1982).

(9) - S. B. Oseroff, R. Calvo and W. Giriat, Z. Fisk. Sol. State Comm. 35, 559 (1980).

(10) - R. R. Gałazka, S. Nagata and P. M. Keesom, Phys. Rev. B22, 3344 (1983).

(11) - H. Kett, W. Gebhart, V. Krey and J. K. Furdyna, J. Magnetism and Magnetic Materials 25, 215 (1981).

(12) - M. Escorne and A. Mauger, Phys. Rev. B25, 4674 (1982).

(13) - M. P. Vecchi, W. Giriat and L. Videla, J. Appl. Phys. Letters 38, 99 (1981).

(14) - B. A. Orłowski, Phys. Stat. Sol. B95, K31 (1979); C. Webb, M. Kaminska, M. Lichtensteiger and J. Lagowski, Sol. State Comm. 40, 609 (1981).

(15) - P. Oelhafen, M. P. Vecchi, J. L. Freeouf and V. L. Moruzzi, Sol. State Comm. 44, 1547 (1982).

(16) - R. R. Gałazka, Physics of Semiconductors 1978, Ed. by B. L. H. Wilson (The Institute of Physics, Bristol, 1979), pag. 133.

(17) - S. Venengopalau, A. Petrou, R. R. Gałazka and A. K. Radamas, Sol. State Comm. 35, 401 (1980).

(18) - M. Zimnal-Starnawska, Ph. D. Thesis, Jagellonian University, Krakow 1980 (unpublished).

(19) - J. C. Mikkelsen and J. B. Boyce, Phys. Rev. Letters 49, 1412 (1982); Phys. Rev. B28, 7130 (1983).

(20) - J. Azoulay, E. A. Stern, D. Shalteil and A. Grayewski, Phys. Rev. B25, 5627 (1982).

(21) - F. Antonangeli, A. Balzarotti, N. Motta, M. Piacentini, A. Kisiel, M. Zimnal-Starnawska and W. Giriat, in "EXAFS and Near Edge Structure", ed. by A. Bianconi, L. Incoccia and S. Stipcich (Springer Verlag, 1983), pag. 224.

(22) - A. Balzarotti, M. T. Czyzyk, A. Kiesel, N. Motta, M. Podgorny and M. Zimnal-Starnawska, (Submitted to Phys. Rev.).

(23) - T. Kendelewicz, Sol. State Comm. 36, 127 (1980).

(24) - M. Zimnal-Starnawska, M. Podgorny, A. Kisiel, W. Giriat, M. Demianiuk and J. Zmija, J. Phys. C17, 615 (1984).

(25) - M. T. Czyzyk and M. Podgorny, Proceedings Conf. on Physics of Semiconductor Compounds, Jaszowiec 1983, Proc. Conf. in Physics, Vol. 5 (Ossolineum, Wrocław, 1984).

(26) - A. Balzarotti, M. De Crescenzi and L. Incoccia, Phys. Rev. B25, 6349 (1982).

(27) - P. A. Lee, P. H. Citrin, P. Eisemberger and B. M. Kincaid, Rev. Mod. Phys. 53, 769 (1981); T. M. Hayes and J. B. Boyce, Solid State Physics, ed. by F. Seitz, D. Turnbull and H. Ehrenreich (Academic Press, 1982), Vol. 37, pag. 173.

(28) - B. K. Teo and P. A. Lee, J. Am. Chem. Soc. 101, 2315 (1979).

(29) - E. A. Stern, B. A. Bunker and S. M. Heald, Phys. Rev. B21, 5521 (1980).

(30) - R. F. Pettifer, in "Inner-Shell and X-Ray Physics of Atoms and Solids", ed. by D. J. Fabian, H. Kleinpoppen and L. M. Watson (Plenum Press, 1980).

(31) - Although our model does not exclude the possibility of clustering of Mn atoms, this particular conclusion is obtained ignoring eventual correlations between different tetrahedra. However, we believe that such a correlation may only slightly change the figures given in the text.

(32) - P. N. Keating, Phys. Rev. 145, 637 (1966).

(33) - M. J. P. Musgrave and J. A. Pople, Proc. Royal Soc. A268, 474 (1962).

(34) - R. M. Martin, Phys. Rev. B1, 4005 (1970).

(35) - R. E. Behringer, J. Chem. Phys. 29, 537 (1958).

(36) - T. M. Hayes, J. W. Hallen, J. B. Boyce and J. J. Hauser, Phys. Rev. B22, 4503 (1980).

(37) - J. C. Phillips, Bonds and Bands in Semiconductors (Academic Press, 1973), and references therein.

(38) - L. Pauling, The Nature of the Chemical Bond (Cornell Univ. Press, 1960).

(39) - H. Franzen and C. Sterner, J. Solid State Chem. 25, 227 (1978).

(40) - J. W. Allen, G. Lucovsky and J. C. Mikkelsen Jr., Solid State Comm. 24, 367 (1977).